Chemical Science

ROYAL SOCIETY OF CHEMISTRY

EDGE ARTICLE

View Article Online
View Journal | View Issue

Cite this: *Chem. Sci.*, 2023, **14**, 3642

All publication charges for this article have been paid for by the Royal Society of Chemistry

Received 15th January 2023
Accepted 5th March 2023

DOI: 10.1039/d3sc00251a

rsc.li/chemical-science

An iodide-containing covalent organic framework for enhanced radiotherapy†

Le-Le Zhou,‡[a] Qun Guan,‡[a] Wei Zhou,[b] Jing-Lan Kan[a] and Yu-Bin Dong*[a]

Metal-free radiosensitizers, particularly iodine, have shown promise in enhancing radiotherapy due to their suitable X-ray absorption capacities and negligible biotoxicities. However, conventional iodine compounds have very short circulating half-lives and are not retained in tumors very well, which significantly limits their applications. Covalent organic frameworks (COFs) are highly biocompatible crystalline organic porous materials that are flourishing in nanomedicine but have not been developed for radiosensitization applications. Herein, we report the room-temperature synthesis of an iodide-containing cationic COF by the three-component one-pot reaction. The obtained **TDI-COF** can be a tumor radiosensitizer for enhanced radiotherapy by radiation-induced DNA double-strand breakage and lipid peroxidation and inhibits colorectal tumor growth by inducing ferroptosis. Our results highlight the excellent potential of metal-free COFs as radiotherapy sensitizers.

Introduction

More than half of the cancer patients are subjected to radiotherapy at some timepoint during disease progression; this technique uses high-energy X-rays to damage cancer cells, and is one of the most cost-effective cancer treatment options.[1] However, the dose and efficacy of radiotherapy are limited by normal tissue toxicity.[2] Radiosensitizers concentrate radiation energy within cancerous tissue or destroy tumor resistance to X-rays, which can improve the efficacy of radiotherapy without increasing the radiation dose, and potentially enhance the radiotherapeutic window, particularly for malignancies with high risks of regional recurrence, such as gastrointestinal cancers.[3] Despite extensive (pre)clinical data that demonstrate the radiosensitizing properties of chemotherapeutic drugs, the intolerable side effects of chemotherapy are clinically limiting its applications.[4–6]

Nanoparticles containing high-*Z* elements, such as Au nanoparticles,[7–11] Bi(III) chalcogenides,[12–15] and metal–organic frameworks (MOFs),[16–20] have recently been used as radiosensitizers. While these inorganic nanomaterials provide large X-ray absorption cross-sections that amplify the radiation energy deposited in tumor tissue and improve radiobiological effects, their biosafety has been questioned.[21] Hence, there is an urgent need to develop metal-free radiosensitizers that are highly biocompatible; in this regard, iodine compounds are noteworthy candidates.[22–24] For example, iopromide and iohexol have high X-ray absorption capacities but are suitable for computed tomography (CT) imaging rather than radiosensitization due to poor vessel-wall penetration, extremely short circulatory half-lives, and low tumor retention.

Covalent organic frameworks (COFs), which are crystalline porous polymeric materials with well-defined chemical structures,[25–30] have attracted extensive research interest in the tumor nanomedicine field, and have been used in drug delivery,[31–36] phototherapy,[37–46] and immunotherapy[47–52] because they are versatile and biocompatible. Recently, AgI@COF-TpBpy was used as a delivery vehicle for radioiodine in brachytherapy, showing a long tumor retention time and effective cancer cell killing performance;[53] however, to our knowledge, the potential of a metal-free COF itself as a radiosensitizer in radiotherapy has not been exploited.[54–56]

In this contribution, we reported a cationic COF with iodide counterions prepared by a three-component *in situ* reaction.[57] The generated **TDI-COF** can be a tumor radiosensitizer to enhance colorectal cancer radiotherapy (Fig. 1). The good X-ray absorption capacity of **TDI-COF** allowed it to promote radiation-induced DNA damage and lipid peroxidation, and induce ferroptosis that inhibits cell proliferation and tumor growth. To our knowledge, this study is not only the first example of metal-free COFs for radiotherapy, but also highlights their great potential as radiotherapy radiosensitizers.

[a]*College of Chemistry, Chemical Engineering and Materials Science, Collaborative Innovation Center of Functionalized Probes for Chemical Imaging in Universities of Shandong, Key Laboratory of Molecular and Nano Probes, Ministry of Education, Shandong Normal University, Jinan 250014, China. E-mail: yubindong@sdnu.edu.cn*
[b]*Department of Oncology, Shandong Provincial Hospital Affiliated to Shandong First Medical University, Jinan 250021, China*

† Electronic supplementary information (ESI) available: Atomic coordinates of the AA- and AB-stacking modes of **TDI-COF** (Tables S1 and S2); supplementary data for material characterization, *in vitro* antitumor experiments, and animal experiments (Fig. S1–S7); and experimental procedures. See DOI: https://doi.org/10.1039/d3sc00251a

‡ These authors contributed equally.

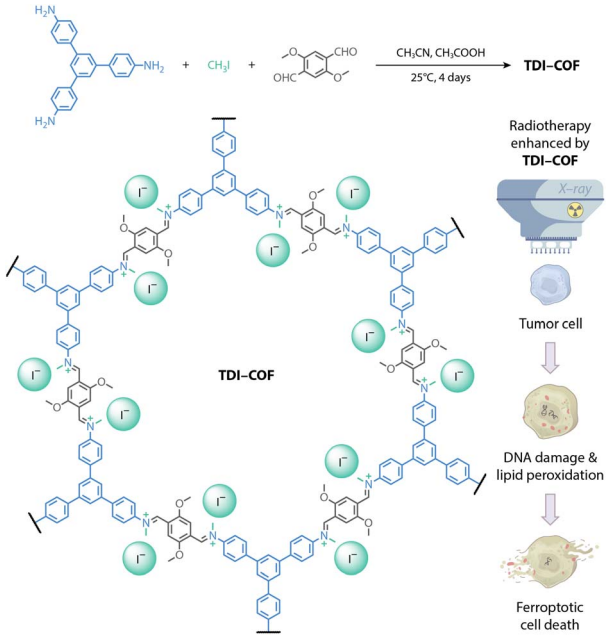

Fig. 1 Synthesis of an iodide-containing and iminium-linked **TDI-COF** as a radiosensitizer for improving radiotherapy efficacy *via* iodide-promoted X-ray deposition.

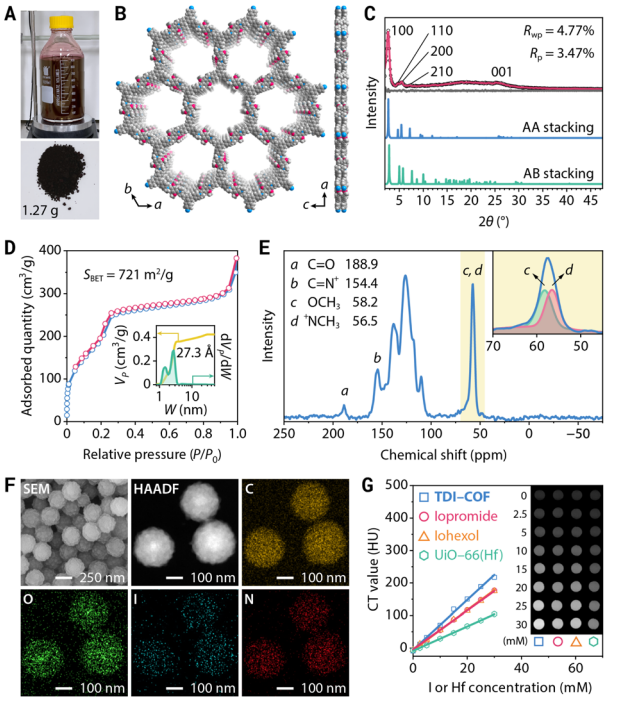

Fig. 2 Synthesis and characterization of **TDI-COF**. (A) Gram-scale synthesis of **TDI-COF**. (B) Top and side views of the crystal structure of **TDI-COF**. (C) Experimental (black dots), Pawley-refined (red), and simulated (blue and green) PXRD patterns and difference plot (gray). (D) N_2 adsorption–desorption isotherm. Inset: cumulative pore volume profile (yellow) and pore size distribution (green). (E) ^{13}C CP-MAS NMR spectrum and deconvolution. (F) SEM and HAADF-STEM images and elemental maps. (G) CT images and the corresponding attenuation plots.

Results and discussion

TDI-COF, which is linked through iminium moieties,[58] was prepared by the one-pot *in situ* reaction of 1,3,5-tris(4-aminophenyl)benzene (TPB), iodomethane, and 2,5-dimethoxyterephthalaldehyde (DMTP) in acetonitrile with acetic acid at 25 °C for 4 days (Fig. 2A). The formation of a model compound of *N*-benzylidene-*N*-methylbenzenaminium iodide in acetonitrile solution implied the rationality of the polymerization reaction (Fig. S1A, ESI†). Inductively coupled plasma–mass spectrometry (ICP-MS) and elemental analysis revealed that **TDI-COF** contains 36.7 ± 1.3 wt% iodine, which is consistent with the $C_{78}H_{60}N_6O_6(CH_3I)_{5.8}$ composition and is very close to the theoretical $C_{78}H_{60}N_6O_6(CH_3I)_6$ formula (Fig. S1B, ESI†).

The crystal structure of **TDI-COF** was determined by powder X-ray diffractometry (PXRD) in combination with computational simulations using the Forcite module in *BIOVIA Materials Studio 2018* to build an initial model,[59–61] followed by density functional based tight binding (DFTB+) calculations to optimize the conformation of the 2D layer and the stacking mode (Fig. 2B).[62–64] The structure of **TDI-COF** was built with the **hcb** topology in space group *P*3 (No. 143) and was further refined from the PXRD pattern by Pawley refinement (Fig. 2C). The layers are stacked in an eclipsed AA mode (Table S1, ESI†), with cell parameters $a = b = 37.45$ Å, $c = 3.46$ Å, $\alpha = \beta = 90°$, and $\gamma = 120°$, and good agreement factors ($R_p = 3.47\%$ and $R_{wp} = 4.77\%$). In contrast, the simulated diffraction pattern of the staggered AB-stacking model deviates from the experimental data for the (100), (110), (200), and (001) peaks, eliminating the AB-stacking structure (Table S2, ESI†).

Furthermore, its permanent porosity was determined by the N_2 adsorption–desorption isotherm acquired at 77 K; the distinct step observed at $P/P_0 = 0.18$–0.26 is the result of mesopore filling and is consistent with a type IV isotherm (Fig. 2D). The Brunauer–Emmett–Teller (BET) surface area was determined to be $S_{BET} = 721$ m^2 g^{-1} with a total pore volume of 0.42 cm^3 g^{-1}. The pore size distribution of **TDI-COF** calculated by nonlocal density functional theory revealed cylindrical pores that are 2.73 nm in diameter,[65] in good agreement with its simulated crystal structure, and micropores with a diameter of 1.48 nm that may be associated with local bonding defects and disorder stacking structures.[66,67] Notably, the cumulative pore volume profile of **TDI-COF** indicated that the contribution of the 2.73 nm mesopore is greater than that of the 1.48 nm micropore, indicating the predominance of the mesopore and the satisfactory structural integrity of **TDI-COF** (Fig. 2D).

The chemical structure of **TDI-COF** was clearly identified by comparison with the unmethylated imine-linked TPB-DMTP-COF produced from TPB and DMTP (Fig. S1C and D, ESI†).[68] The iminium C of **TDI-COF** was observed at 154.4 ppm in its ^{13}C cross-polarization-magic angle spinning nuclear magnetic resonance (CP-MAS NMR) spectrum, fully confirming the formation of an iminium linkage (Fig. 2E). The nonexistent imine C (149.4 ppm) and very weak aldehyde C (188.9 ppm)

characteristic peaks are again indicative of a high-yield iminium formation (Fig. S1E, ESI†). The methyl C signal was deconvoluted into two peaks with nearly identical intensities that respectively correspond to N^+CH_3 (56.5 ppm) and OCH_3 (58.2 ppm). The formation of the iminium linkage was further supported by Fourier-transform infrared spectroscopy, with a characteristic C=N^+ stretching vibration at 1645 cm^{-1} and negligible peaks of the residual CHO and C=N at 1682 and 1617 cm^{-1}, respectively (Fig. S1F, ESI†).[69] Furthermore, the high-resolution N 1s X-ray photoelectron spectroscopy (XPS) profile showed a symmetrical peak at 401.2 eV that further evidenced the formation of a C=N^+ moiety (Fig. S1G, ESI†). In addition, two XPS peaks associated with I^- are located at 619.3 and 630.8 eV, with a well-separated 11.5 eV spin–orbit component, and no impurity peaks associated with IO_3^-, C–I bonds, or polyiodide species (*e.g.*, I_3^- and I_5^-) were detected, confirming that the only form of iodine present is I^- (Fig. S1H, ESI†).[70,71] Consistent with this, the characteristic stretching vibration bands of the polyiodide species were also not detected in the Raman spectrum of **TDI-COF** (Fig. S1I, ESI†).[72] Thermogravimetric analysis showed that **TDI-COF** is thermally stable up to approximately 280 °C, demonstrating the absence of I_2 species in the pores (Fig. S1J, ESI†).

Transmission electron microscopy (TEM) and scanning electron microscopy (SEM) images revealed that **TDI-COF** possesses a uniform nanospherical morphology with a particle size of 243 ± 13 nm (Fig. S1K and L, ESI†). High-resolution TEM images revealed rough nanoparticles composed of small flakes, with well-defined lattice fringes (Fig. S1M, ESI†). The fast Fourier transform of the selected area showed a twofold symmetric pattern with the expected repeat distance of 0.34 nm, which is consistent with the π–π stacking distance calculated from the simulated AA-stacking structure (Fig. S1N, ESI†). In addition, selected area electron diffraction patterns showed a diffraction ring that was indexed to the (001) plane, revealing the acceptable crystallinity and the polycrystalline nature of **TDI-COF** (Fig. S1O, ESI†). High-angle annular dark-field scanning transmission electron microscopy (HAADF-STEM) and element maps indicated that C, O, I, and N are uniformly distributed in the nanoparticles (Fig. 2F). Moreover, time-dependent dynamic light scattering, zeta potential analysis, and PXRD measurements showed that **TDI-COF** has good dispersibility and chemical stability in phosphate-buffered saline (PBS), RPMI-1640 medium, and fetal bovine serum (Fig. S2, ESI†).

The high iodide content endows **TDI-COF** with an effective X-ray absorption capacity that was assessed by CT, which revealed a good linear relationship between the CT value and the **TDI-COF** iodide concentration in PBS. The obtained specific CT value of 7.69 ± 0.19 HU mM^{-1} (I equiv.) is clearly higher than those of iopromide (5.97 ± 0.06 HU mM^{-1}) and iohexol (6.15 ± 0.04 HU mM^{-1}), which are clinical CT contrast media, and significantly higher than that of UiO-66(Hf), a Hf-based MOF with a CT value of 3.75 ± 0.05 HU mM^{-1} (Hf equiv.) (Fig. 2G).[73–75]

Due to its nanoscale size and electropositive framework, **TDI-COF** enters tumor cells through energy-dependent pinocytosis (Fig. S3A, ESI†).[76] Iodide ions attached to the **TDI-COF** crystalline framework exhibit better membrane permeability than iodinated CT contrast agents and free iodide ions (Fig. S3B, ESI†). This is because the cellular uptake of **TDI-COF** is independent of ion transporters[77] and to some extent bypasses the homeostatic regulation of anions. Notably, **TDI-COF** was observed to increase X-ray deposition in tumor cells, thereby enhancing cellular damage. Specifically, HCT-116 colorectal cancer cells treated with **TDI-COF** and subsequently exposed to X-rays exhibited significantly altered morphologies (Fig. 3A), including swelling, enlarged and vacuolated nuclei, and increased lipid droplet numbers, consistent with previous reports.[78–80] Cell viability assays further revealed that cell damage depended on the **TDI-COF** concentration and X-ray dose (Fig. 3B). In clonogenic assays, **TDI-COF** consistently showed improved radiotherapy performance, suppressing both the number and size of the formed cell colonies more significantly than X-ray exposure alone (Fig. 3C). Moreover, **TDI-COF** pretreatment and subsequent 4 Gy X-ray radiation almost completely inhibited the ability of HCT-116 cells to form multicellular spheres under 3D-culture conditions, demonstrating the potentiating effect of **TDI-COF** as a radiosensitizer toward X-ray-induced cell damage (Fig. 3D). Notably, **TDI-COF** affected cells negligibly in the absence of X-rays, highlighting its high biosafety.

The cell death mechanism induced by **TDI-COF**-enhanced radiotherapy was next explored. As a highly sensitive and specific biomarker for early-stage DNA double-strand breakage,[81] γH2AX, the Ser139-phosphorylated product of H2A histone family member X, is more highly expressed in HCT-116 cells co-treated with **TDI-COF** and X-rays than in HCT-116 cells treated with X-rays alone, from which we reasoned that **TDI-COF** could increase DNA damage caused by radiotherapy (Fig. 3E). Liperfluo and 2′,7′-dichlorodihydrofluorescein diacetate (DCFH-DA) staining revealed that the **TDI-COF** treatment respectively increased the levels of intracellular lipid peroxides and reactive oxygen species (ROS) upon X-ray radiation, especially under high-dose conditions, indicative of redox dyshomeostasis (Fig. 3F and S4A, ESI†).[82,83] In addition, we also examined ferroptosis-related protein expression given the close relationship between lipid peroxidation and ferroptosis (Fig. 3G).[84,85] As a result, radiotherapy led to a decreased glutathione peroxidase 4 (GPX4) level, consistent with the central regulatory defense mechanism against cell ferroptosis,[86,87] which was further exacerbated by **TDI-COF**. Interestingly, co-treatment with **TDI-COF** and X-rays also slightly decreased the expression of solute carrier family 7 member 11 (SLC7A11), which regulated ferroptosis by translocating extracellular cystine into cells.[88] GPX4 and SLC7A11 downregulation are both contributing factors for ferroptosis. Radiotherapy negligibly affected the level of acyl-coenzyme A synthetase long-chain family member 4 (ACSL4).[89] The intracellular level of glutathione (GSH), a major antioxidant, decreased consistently with increasing X-ray dose and was further downregulated by **TDI-COF** treatment (Fig. 3H). Levels of malondialdehyde, a lipid-peroxide breakdown product and a biochemical marker of ferroptosis,[90] were significantly

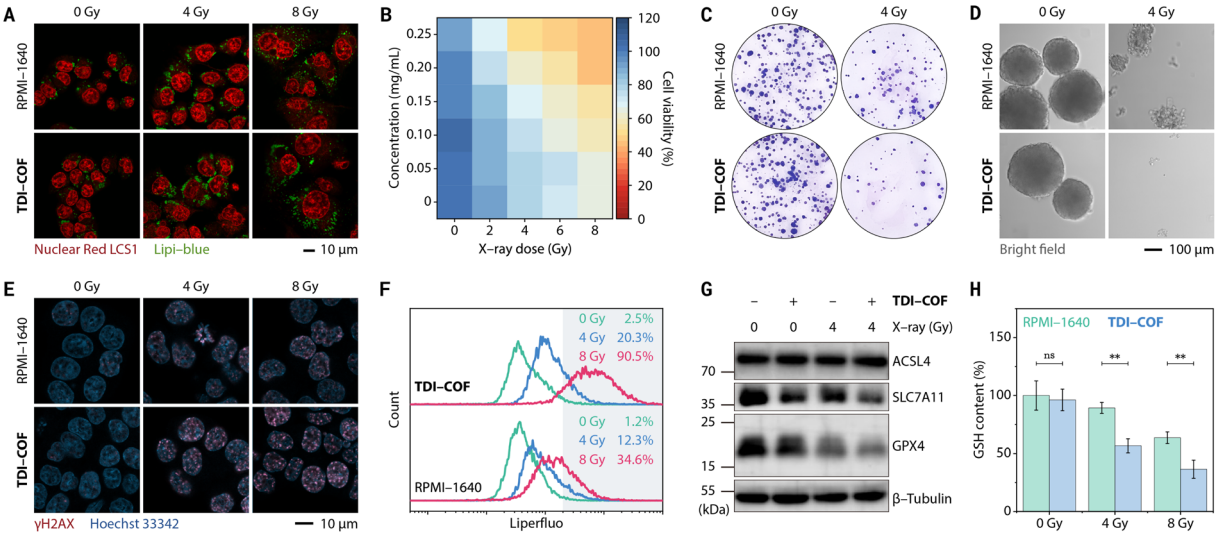

Fig. 3 Ferroptosis-related radiotherapy of HCT-116 cells pretreated with TDI-COF (0–0.25 mg mL^{-1}) for 4 h and exposed to X-ray radiation (0–8 Gy). (A) Confocal laser scanning microscopy images showing cellular morphological changes and increased lipid droplet numbers. (B) CCK-8 cell viability assay. (C) Clonogenic assay. (D) Multicellular tumor spheroid formation assay. (E) Confocal laser scanning microscopy images following γH2AX immunofluorescence staining. (F) Flow cytometric analysis of intracellular lipid peroxides. (G) Western blots of ferroptosis-related proteins. (H) Intracellular GSH levels. Data are presented as means ± SDs ($n = 3$) and compared by two-way analysis of variance (ANOVA) followed by Bonferroni's multiple comparison test. $^{**}p < 0.01$; ns, no significance ($p > 0.05$).

higher after radiotherapy (Fig. S4B, ESI†). As expected, **TDI-COF** treatment alone did not alter GSH and malondialdehyde levels. Furthermore, **TDI-COF**-enhanced radiotherapy failed to activate caspase 3 under the same conditions, suggesting that an apoptotic mechanism is not involved in cell death (Fig. S4C, ESI†). The ferroptosis mechanism was further evidenced in cell rescue experiments (Fig. S4D and E, ESI†). Glutathione ethyl ester (a cell-permeable reducing agent), *N*-acetylcysteine (a GSH biosynthesis raw material), ferrostatin-1 (a ferroptosis inhibitor), and deferoxamine mesylate (an iron chelator) were able to restore cell viability after **TDI-COF**-enhanced radiotherapy, irrespective of the X-ray dose (4 or 8 Gy), whereas Z-VAD-FMK (an apoptosis inhibitor), necrostatin-1s (a necroptosis inhibitor), or 3-methyladenine (an autophagy inhibitor) did not, which fully supports a ferroptosis mechanism.[91]

In addition to colorectal cancer, **TDI-COF** also enhanced radiotherapy for breast cancer (Fig. S5A and B, ESI†), even at very low X-ray doses (*e.g.*, 2 Gy). Experiments have shown that MCF-7 cell death involves ferroptosis (but other cell death mechanisms cannot be completely excluded) and is closely associated with oxidative stress caused by DNA damage and GSH depletion (Fig. S5C–G, ESI†).

The tumor retention time of radiosensitizers is critical for enhancing X-ray deposition at the tumor sites.[92] The tumor retention with a half-life of approximately 4 h after intratumoral injection of **TDI-COF** into HCT-116 tumor-bearing nude mice was significantly higher than that of iopromide (<2 h), which may be related to the enhanced permeability and retention (EPR) effect (Fig. S6A, ESI†).[93] **TDI-COF** was primarily excreted through urine 72 h after the injection (Fig. S6B, ESI†), with an excretion rate of 64.9 ± 10.4%, which was comparable to that of iopromide (78.6 ± 13.4%) but obviously higher than that of UiO-66(Hf) (30.2 ± 15.4%). As a result, **TDI-COF** has acceptable intratumoral retention and low residue *in vivo*, resulting in minimum potential toxicity while assuring the effectiveness of tumor radiotherapy.

Encouraged by the remarkable efficacy of **TDI-COF**, its good *in vitro* biocompatibility and *in vivo* long tumor retention, we next examined its efficacy in *in vivo* radiotherapy (Fig. 4A). Tumors injected intratumorally with **TDI-COF** and exposed to low doses of X-rays were almost completely suppressed after 16 days, while tumors treated with X-rays alone showed only slightly lower growth rates (Fig. 4B–D). Tumors pathologically analyzed following treatment exhibited trends consistent with the tumor growth curves (Fig. 4E). Hematoxylin–eosin (H&E) staining revealed that a high percentage of cells in the group treated with **TDI-COF** and exposed to X-rays exhibited ferroptosis- and necrosis-like damage characterized by karyorrhexis, karyopyknosis, and ruptured plasma membranes.[94] Immunohistochemical staining showed that the level of Ki67, a proliferative and prognostic marker,[95] was consistently significantly lower in the group receiving **TDI-COF**-enhanced radiotherapy than in the group receiving radiotherapy alone. In addition, the almost no weight loss observed during radiotherapy suggests that **TDI-COF** is biosafe (Fig. 4F). Histological analysis of H&E stains of the major organs obtained at the treatment endpoint showed that there was no obvious abnormality of pathological observation, further supporting the biocompatibility of **TDI-COF** (Fig. S7, ESI†). In brief, these preliminary results underscore the *in vivo* effectiveness and biocompatibility of the **TDI-COF** radiosensitizer.

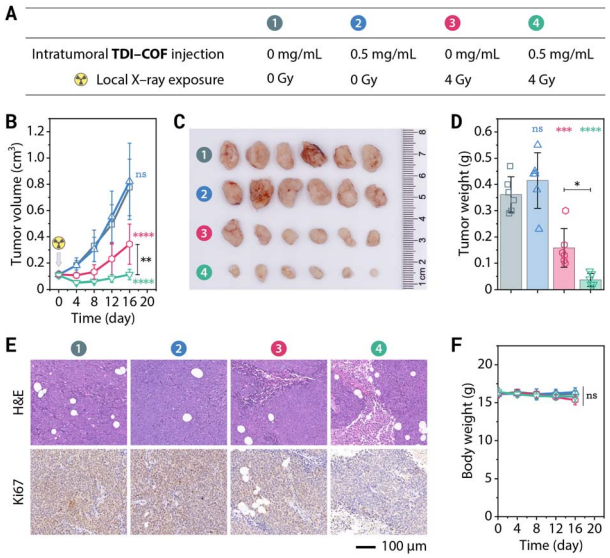

Fig. 4 TDI-COF-enhanced radiotherapy in HCT-116 tumor-bearing nude mice. (A) Therapeutic schedule. (B) Tumor growth curves. (C) Weights of tumor tissue obtained by dissection. (D) Photographic images of the obtained tumors at the treatment endpoint. (E) Representative H&E and Ki67 staining images of the tumor tissue sampled at the treatment endpoint. (F) Body weight curves. Data are presented as means ± SDs (n = 6) and compared by two-way ANOVA followed by Tukey's *post hoc* test (B, F) and one-way ANOVA followed by Tukey's *post hoc* test (D). ****p < 0.0001; ***p < 0.001; **p < 0.01; *p < 0.05; *ns*, no significance (p > 0.05).

Conclusions

In conclusion, we synthesized an iodide-containing and iminium-linked COF by a three-component one-pot *in situ* reaction at room temperature. The generated **TDI-COF** significantly improved X-ray deposition in colorectal cancer cells, effectively sensitized low-dose X-ray-induced radiotherapy, triggered ferroptotic cell death by damaging DNA and promoting lipid peroxidation, and displayed potent *in vitro* and *in vivo* antitumor activities as a consequence. Although further laboratorial and preclinical experiments including targeted delivery, catabolic pathways, and genotoxicity are necessary, our study demonstrated that metal-free COFs can be potential sensitizers for enhancing radiotherapy and possibly provide a new method for developing COF-based oncotherapies.

Author contributions

Conceptualization, Y.-B. Dong. Investigation, L.-L. Zhou, Q. Guan, and W. Zhou. Software, J.-L. Kan. Methodology, L.-L. Zhou, Q. Guan, and Y.-B. Dong. Project administration, Y.-B. Dong. Resources, Y.-B. Dong. Supervision, Y.-B. Dong. Visualization, Q. Guan. Writing – original draft, L.-L. Zhou and Q. Guan. Writing – review & editing, L.-L. Zhou, Q. Guan, and Y.-B. Dong.

Data availability

The data that support the findings of this study are presented in the paper and the ESI.†

Conflicts of interest

There are no conflicts to declare.

Acknowledgements

All animal experiments complied with the relevant guidelines of the Chinese government and regulations for the care and use of experimental animals under approval number AEECSDNU2021009 by the Ethics Committee of Shandong Normal University (Jinan, China). The authors acknowledge financial support from the National Natural Science Foundation of China (Grant No. 21971153), the Major Basic Research Projects of the Shandong Provincial Natural Science Foundation (No. ZR2020ZD32), and the Taishan Scholars Climbing Program of Shandong Province.

References

1 D. E. Citrin, Recent Developments in Radiotherapy, *New Engl. J. Med.*, 2017, **377**, 1065–1075, DOI: **10.1056/NEJMra1608986**.

2 M. I. Khan, F. Batool, R. Ali, Q. u. A. Zahra, W. Wang, S. Li, G. Wang, L. Liu, S. U. Khan, M. Mansoor, M. Bilal, W. Ding, A. Kazmi, F. Li and B. Qiu, Tailoring Radiotherapies and Nanotechnology for Targeted Treatment of Solid Tumors, *Coord. Chem. Rev.*, 2022, **472**, 214757, DOI: **10.1016/j.ccr.2022.214757**.

3 S. Bonvalot, P. L. Rutkowski, J. Thariat, S. Carrère, A. Ducassou, M.-P. Sunyach, P. Agoston, A. Hong, A. Mervoyer, M. Rastrelli, V. Moreno, R. K. Li, B. Tiangco, A. C. Herraez, A. Gronchi, L. Mangel, T. Sy-Ortin, P. Hohenberger, T. de Baère, A. Le Cesne, S. Helfre, E. Saada-Bouzid, A. Borkowska, R. Anghel, A. Co, M. Gebhart, G. Kantor, A. Montero, H. H. Loong, R. Vergés, L. Lapeire, S. Dema, G. Kacso, L. Austen, L. Moureau-Zabotto, V. Servois, E. Wardelmann, P. Terrier, A. J. Lazar, J. V. M. G. Bovée, C. Le Péchoux and Z. Papai, NBTXR3, a First-in-Class Radioenhancer Hafnium Oxide Nanoparticle, plus Radiotherapy versus Radiotherapy Alone in Patients with Locally Advanced Soft-Tissue Sarcoma (Act.In.Sarc): A Multicentre, Phase 2–3, Randomised, Controlled Trial, *Lancet Oncol.*, 2019, **20**, 1148–1159, DOI: **10.1016/S1470-2045(19)30326-2**.

4 N. K. Altorki, T. E. McGraw, A. C. Borczuk, A. Saxena, J. L. Port, B. M. Stiles, B. E. Lee, N. J. Sanfilippo, R. J. Scheff, B. B. Pua, J. F. Gruden, P. J. Christos, C. Spinelli, J. Gakuria, M. Uppal, B. Binder, O. Elemento, K. V. Ballman and S. C. Formenti, Neoadjuvant Durvalumab with or without Stereotactic Body Radiotherapy in Patients with Early-Stage Non-Small-Cell Lung Cancer: A Single-Centre, Randomised Phase 2 Trial, *Lancet Oncol.*, 2021, **22**, 824–835, DOI: **10.1016/S1470-2045(21)00149-2**.

5 C. M. S. Tesileanu, M. Sanson, W. Wick, A. A. Brandes, P. M. Clement, S. C. Erridge, M. A. Vogelbaum, A. K. Nowak, J.-F. Baurain, W. P. Mason, H. Wheeler,

O. L. Chinot, S. Gill, M. Griffin, L. Rogers, W. Taal, R. Rudà, M. Weller, C. McBain, M. E. van Linde, K. Aldape, R. B. Jenkins, J. M. Kros, P. Wesseling, A. von Deimling, Y. Hoogstrate, I. de Heer, P. N. Atmodimedjo, H. J. Dubbink, R. W. W. Brouwer, W. F. J. van Ijcken, K. J. Cheung, V. Golfinopoulos, B. G. Baumert, T. Gorlia, P. J. French and M. J. van den Bent, Temozolomide and Radiotherapy versus Radiotherapy Alone in Patients with Glioblastoma, IDH-wildtype: Post Hoc Analysis of the EORTC Randomized Phase III CATNON Trial, *Clin. Cancer Res.*, 2022, **28**, 2527–2535, DOI: **10.1158/1078-0432.CCR-21-4283**.

6 S. Kim, E. Wuthrick, D. Blakaj, Z. Eroglu, C. Verschraegen, R. Thapa, M. Mills, K. Dibs, C. Liveringhouse, J. Russell, J. J. Caudell, A. Tarhini, J. Markowitz, K. Kendra, R. Wu, D.-T. Chen, A. Berglund, L. Michael, M. Aoki, M.-H. Wang, I. Hamaidi, P. Cheng, J. de la Iglesia, R. J. Slebos, C. H. Chung, T. C. Knepper, C. M. Moran-Segura, J. V. Nguyen, B. A. Perez, T. Rose, L. Harrison, J. L. Messina, V. K. Sondak, K. Y. Tsai, N. I. Khushalani and A. S. Brohl, Combined Nivolumab and Ipilimumab with or without Stereotactic Body Radiation Therapy for Advanced Merkel Cell Carcinoma: A Randomised, Open Label, Phase 2 Trial, *Lancet*, 2022, **400**, 1008–1019, DOI: **10.1016/S0140-6736(22)01659-2**.

7 L. Wang, W. Jiang, L. Xiao, H. Li, Z. Chen, Y. Liu, J. Dou, S. Li, Q. Wang, W. Han, Y. Wang and H. Liu, Self-Reporting and Splitting Nanopomegranates Potentiate Deep Tissue Cancer Radiotherapy via Elevated Diffusion and Transcytosis, *ACS Nano*, 2020, **14**, 8459–8472, DOI: **10.1021/acsnano.0c02674**.

8 M. Yuan, X. Fang, Y. Wu, Y. Xu, H. Feng, J. Mu, Z. Chen, Y. Lin, Q. Fu, W. Du, H. Yang and J. Song, Activatable Nanoprobe with Aggregation-Induced Dual Fluorescence and Photoacoustic Signal Enhancement for Tumor Precision Imaging and Radiotherapy, *Anal. Chem.*, 2022, **94**, 5204–5211, DOI: **10.1021/acs.analchem.2c00340**.

9 Y. Yang, M. Chen, B. Wang, P. Wang, Y. Liu, Y. Zhao, K. Li, G. Song, X.-B. Zhang and W. Tan, NIR-II Driven Plasmon-Enhanced Catalysis for a Timely Supply of Oxygen to Overcome Hypoxia-Induced Radiotherapy Tolerance, *Angew. Chem., Int. Ed.*, 2019, **58**, 15069–15075, DOI: **10.1002/anie.201906758**.

10 T.-T. Jia, B.-J. Li, G. Yang, Y. Hua, J.-Q. Liu, W. Ma, S.-Q. Zang, X. Chen and X. Zhao, Enantiomeric Alkynyl-Protected Au10 Clusters with Chirality-Dependent Radiotherapy Enhancing Effects, *Nano Today*, 2021, **39**, 101222, DOI: **10.1016/j.nantod.2021.101222**.

11 Z. He, X. Huang, C. Wang, X. Li, Y. Liu, Z. Zhou, S. Wang, F. Zhang, Z. Wang, O. Jacobson, J.-J. Zhu, G. Yu, Y. Dai and X. Chen, A Catalase-Like Metal-Organic Framework Nanohybrid for O2-Evolving Synergistic Chemoradiotherapy, *Angew. Chem., Int. Ed.*, 2019, **58**, 8752–8756, DOI: **10.1002/anie.201902612**.

12 Z. Song, T. Liu, H. Lai, X. Meng, L. Yang, J. Su and T. Chen, A Universally EDTA-Assisted Synthesis of Polytypic Bismuth Telluride Nanoplates with a Size-Dependent Enhancement of Tumor Radiosensitivity and Metabolism In Vivo, *ACS Nano*, 2022, **16**, 4379–4396, DOI: **10.1021/acsnano.1c10663**.

13 X. Wang, Z. Guo, C. Zhang, S. Zhu, L. Li, Z. Gu and Y. Zhao, Ultrasmall BiOI Quantum Dots with Efficient Renal Clearance for Enhanced Radiotherapy of Cancer, *Adv. Sci.*, 2020, **7**, 1902561, DOI: **10.1002/advs.201902561**.

14 Y. Kang, X. Yu, X. Fan, Aodenggerile, S. Zhao, C. Tu, Z. Yan, R. Wang, W. Li and H. Qiu, Tetramodal Imaging and Synergistic Cancer Radio-Chemotherapy Enabled by Multiple Component-Encapsulated Zeolitic Imidazolate Frameworks, *ACS Nano*, 2020, **14**, 4336–4351, DOI: **10.1021/acsnano.9b09858**.

15 X. Huang, F. Zha, J. Zou, Y. Li, F. Wang and X. Chen, Photoacoustic Imaging-Guided Synergistic Photothermal/Radiotherapy Using Plasmonic Bi/Bi2O3−x Nanoparticles, *Adv. Funct. Mater.*, 2022, **32**, 2113353, DOI: **10.1002/adfm.202113353**.

16 G. Lan, K. Ni, S. S. Veroneau, T. Luo, E. You and W. Lin, Nanoscale Metal–Organic Framework Hierarchically Combines High-Z Components for Multifarious Radio-Enhancement, *J. Am. Chem. Soc.*, 2019, **141**, 6859–6863, DOI: **10.1021/jacs.9b03029**.

17 N. Guo, K. Ni, T. Luo, G. Lan, A. Arina, Z. Xu, J. Mao, R. R. Weichselbaum, M. Spiotto and W. Lin, Reprogramming of Neutrophils as Non-canonical Antigen Presenting Cells by Radiotherapy–Radiodynamic Therapy to Facilitate Immune-Mediated Tumor Regression, *ACS Nano*, 2021, **15**, 17515–17527, DOI: **10.1021/acsnano.1c04363**.

18 T. Luo, G. T. Nash, X. Jiang, X. Feng, J. Mao, J. Liu, A. Juloori, A. T. Pearson and W. Lin, A 2D Nanoradiosensitizer Enhances Radiotherapy and Delivers STING Agonists to Potentiate Cancer Immunotherapy, *Adv. Mater.*, 2022, **34**, 2110588, DOI: **10.1002/adma.202110588**.

19 Z. Xu, T. Luo, J. Mao, C. McCleary, E. Yuan and W. Lin, Monte Carlo Simulation-Guided Design of a Thorium-Based Metal–Organic Framework for Efficient Radiotherapy-Radiodynamic Therapy, *Angew. Chem., Int. Ed.*, 2022, **61**, e202208685, DOI: **10.1002/anie.202208685**.

20 W. Zhou, Z. Liu, N. Wang, X. Chen, X. Sun and Y. Cheng, Hafnium-Based Metal–Organic Framework Nanoparticles as a Radiosensitizer to Improve Radiotherapy Efficacy in Esophageal Cancer, *ACS Omega*, 2022, **7**, 12021–12029, DOI: **10.1021/acsomega.2c00223**.

21 R. Ettlinger, U. Lächelt, R. Gref, P. Horcajada, T. Lammers, C. Serre, P. Couvreur, R. E. Morris and S. Wuttke, Toxicity of Metal–Organic Framework Nanoparticles: From Essential Analyses to Potential Applications, *Chem. Soc. Rev.*, 2022, **51**, 464–484, DOI: **10.1039/D1CS00918D**.

22 K. E. deKrafft, Z. Xie, G. Cao, S. Tran, L. Ma, O. Z. Zhou and W. Lin, Iodinated Nanoscale Coordination Polymers as Potential Contrast Agents for Computed Tomography, *Angew. Chem., Int. Ed.*, 2009, **48**, 9901–9904, DOI: **10.1002/anie.200904958**.

23 B. L. Cline, W. Jiang, C. Lee, Z. Cao, X. Yang, S. Zhan, H. Chong, T. Zhang, Z. Han, X. Wu, L. Yao, H. Wang, W. Zhang, Z. Li and J. Xie, Potassium Iodide Nanoparticles

Enhance Radiotherapy against Breast Cancer by Exploiting the Sodium-Iodide Symporter, *ACS Nano*, 2021, **15**, 17401–17411, DOI: **10.1021/acsnano.1c01435**.

24 M. Yin, X. Liu, Z. Lei, Y. Gao, J. Liu, S. Tian, Z. Liang, Y. Wang, F. Meng and L. Luo, Precisely Translating Computed Tomography Diagnosis Accuracy into Therapeutic Intervention by a Carbon-Iodine Conjugated Polymer, *Nat. Commun.*, 2022, **13**, 2625, DOI: **10.1038/s41467-022-30263-1**.

25 C. S. Diercks and O. M. Yaghi, The Atom, the Molecule, and the Covalent Organic Framework, *Science*, 2017, **355**, eaal1585, DOI: **10.1126/science.aal1585**.

26 O. M. Yaghi, M. J. Kalmutzki and C. S. Diercks, *Introduction to Reticular Chemistry: Metal-Organic Frameworks and Covalent Organic Frameworks*, Wiley-VCH, Weinheim, 2019, DOI: **10.1002/9783527821099**.

27 K. Geng, T. He, R. Liu, S. Dalapati, K. T. Tan, Z. Li, S. Tao, Y. Gong, Q. Jiang and D. Jiang, Covalent Organic Frameworks: Design, Synthesis, and Functions, *Chem. Rev.*, 2020, **120**, 8814–8933, DOI: **10.1021/acs.chemrev.9b00550**.

28 R. Liu, K. T. Tan, Y. Gong, Y. Chen, Z. Li, S. Xie, T. He, Z. Lu, H. Yang and D. Jiang, Covalent Organic Frameworks: An Ideal Platform for Designing Ordered Materials and Advanced Applications, *Chem. Soc. Rev.*, 2021, **50**, 120–242, DOI: **10.1039/D0CS00620C**.

29 Q. Guan, L.-L. Zhou and Y.-B. Dong, Metalated Covalent Organic Frameworks: From Synthetic Strategies to Diverse Applications, *Chem. Soc. Rev.*, 2022, **51**, 6307–6416, DOI: **10.1039/D1CS00983D**.

30 C. Qian, L. Feng, W. L. Teo, J. Liu, W. Zhou, D. Wang and Y. Zhao, Imine and Imine-Derived Linkages in Two-Dimensional Covalent Organic Frameworks, *Nat. Rev. Chem.*, 2022, **6**, 881–898, DOI: **10.1038/s41570-022-00437-y**.

31 V. S. Vyas, M. Vishwakarma, I. Moudrakovski, F. Haase, G. Savasci, C. Ochsenfeld, J. P. Spatz and B. V. Lotsch, Exploiting Noncovalent Interactions in an Imine-Based Covalent Organic Framework for Quercetin Delivery, *Adv. Mater.*, 2016, **28**, 8749–8754, DOI: **10.1002/adma.201603006**.

32 S. Liu, C. Hu, Y. Liu, X. Zhao, M. Pang and J. Lin, One-Pot Synthesis of DOX@Covalent Organic Framework with Enhanced Chemotherapeutic Efficacy, *Chem.–Eur. J.*, 2019, **25**, 4315–4319, DOI: **10.1002/chem.201806242**.

33 Q. Guan, L.-L. Zhou and Y.-B. Dong, Construction of Nanoscale Covalent Organic Frameworks via Photocatalysis-Involved Cascade Reactions for Tumor-Selective Treatment, *Adv. Therap.*, 2022, **5**, 2100177, DOI: **10.1002/adtp.202100177**.

34 W. Zhao, C. Yu, J. Zhao, F. Chen, X. Guan, H. Li, B. Tang, G. Yu, V. Valtchev, Y. Yan, S. Qiu and Q. Fang, 3D Hydrazone-Functionalized Covalent Organic Frameworks as pH-Triggered Rotary Switches, *Small*, 2021, **17**, 2102630, DOI: **10.1002/smll.202102630**.

35 P. Gao, T. Zheng, B. Cui, X. Liu, W. Pan, N. Li and B. Tang, Reversing Tumor Multidrug Resistance with a Catalytically Active Covalent Organic Framework, *Chem. Commun.*, 2021, **57**, 13309–13312, DOI: **10.1039/D1CC04414A**.

36 L. Li, Q. Yun, C. Zhu, G. Sheng, J. Guo, B. Chen, M. Zhao, Z. Zhang, Z. Lai, X. Zhang, Y. Peng, Y. Zhu and H. Zhang, Isoreticular Series of Two-Dimensional Covalent Organic Frameworks with the kgd Topology and Controllable Micropores, *J. Am. Chem. Soc.*, 2022, **144**, 6475–6482, DOI: **10.1021/jacs.2c01199**.

37 Q. Guan, D.-D. Fu, Y.-A. Li, X.-M. Kong, Z.-Y. Wei, W.-Y. Li, S.-J. Zhang and Y.-B. Dong, BODIPY-Decorated Nanoscale Covalent Organic Frameworks for Photodynamic Therapy, *iScience*, 2019, **14**, 180–198, DOI: **10.1016/j.isci.2019.03.028**.

38 Q. Guan, L.-L. Zhou, Y.-A. Li, W.-Y. Li, S. Wang, C. Song and Y.-B. Dong, Nanoscale Covalent Organic Framework for Combinatorial Antitumor Photodynamic and Photothermal Therapy, *ACS Nano*, 2019, **13**, 13304–13316, DOI: **10.1021/acsnano.9b06467**.

39 Q. Guan, L.-L. Zhou, F.-H. Lv, W.-Y. Li, Y.-A. Li and Y.-B. Dong, A Glycosylated Covalent Organic Framework Equipped with BODIPY and CaCO3 for Synergistic Tumor Therapy, *Angew. Chem., Int. Ed.*, 2020, **59**, 18042–18047, DOI: **10.1002/anie.202008055**.

40 L. Zhang, S. Wang, Y. Zhou, C. Wang, X.-z. Zhang and H. Deng, Covalent Organic Frameworks as Favorable Constructs for Photodynamic Therapy, *Angew. Chem., Int. Ed.*, 2019, **58**, 14213–14218, DOI: **10.1002/anie.201909020**.

41 P. Gao, R. Wei, B. Cui, X. Liu, Y. Chen, W. Pan, N. Li and B. Tang, Ultrathin Functionalized Covalent Organic Framework Nanosheets for Tumor-Targeted Photodynamic Therapy, *Chem. Commun.*, 2021, **57**, 6082–6085, DOI: **10.1039/D1CC02124A**.

42 R. Xia, X. Zheng, C. Li, X. Yuan, J. Wang, Z. Xie and X. Jing, Nanoscale Covalent Organic Frameworks with Donor–Acceptor Structure for Enhanced Photothermal Ablation of Tumors, *ACS Nano*, 2021, **15**, 7638–7648, DOI: **10.1021/acsnano.1c01194**.

43 Z. Mi, P. Yang, R. Wang, J. Unruangsri, W. Yang, C. Wang and J. Guo, Stable Radical Cation-Containing Covalent Organic Frameworks Exhibiting Remarkable Structure-Enhanced Photothermal Conversion, *J. Am. Chem. Soc.*, 2019, **141**, 14433–14442, DOI: **10.1021/jacs.9b07695**.

44 X. Wan, T. Wu, L. Song, W. Pan, N. Li and B. Tang, Selenium-Engineered Covalent Organic Frameworks for High-Efficiency and Long-Acting Cancer Therapy, *Chem. Commun.*, 2021, **57**, 6145–6148, DOI: **10.1039/D1CC01830B**.

45 T.-X. Luan, L. Du, J.-R. Wang, K. Li, Q. Zhang, P.-Z. Li and Y. Zhao, Highly Effective Generation of Singlet Oxygen by an Imidazole-Linked Robust Photosensitizing Covalent Organic Framework, *ACS Nano*, 2022, **16**, 21565–21575, DOI: **10.1021/acsnano.2c10423**.

46 Z. Han, Y. Qian, X. Gao, D. Yang, Y. Cai, Y. Chen, J. Jin and Z. Yang, Hypoxia-Responsive Covalent Organic Framework by Single NIR Laser-Triggered for Multimodal Synergistic Therapy of Triple-Negative Breast Cancer, *Colloids Surf., B*, 2023, **222**, 113094, DOI: **10.1016/j.colsurfb.2022.113094**.

47 L.-L. Yang, L. Zhang, S.-C. Wan, S. Wang, Z.-Z. Wu, Q.-C. Yang, Y. Xiao, H. Deng and Z.-J. Sun, Two-Photon Absorption Induced Cancer Immunotherapy Using

Covalent Organic Frameworks, *Adv. Funct. Mater.*, 2021, **31**, 2103056, DOI: 10.1002/adfm.202103056.

48 L. Zhang, L.-L. Yang, S.-C. Wan, Q.-C. Yang, Y. Xiao, H. Deng and Z.-J. Sun, Three-Dimensional Covalent Organic Frameworks with Cross-Linked Pores for Efficient Cancer Immunotherapy, *Nano Lett.*, 2021, **21**, 7979–7988, DOI: 10.1021/acs.nanolett.1c02050.

49 Z. Lu, S. Bai, Y. Jiang, S. Wu, D. Xu, Y. Chen, Y. Lan, Y. An, J. Mao, X. Liu and G. Liu, Porphyrin-Based Covalent Organic Framework for Imaging-Guided Cancer Combinatorial Immuno-Sonodynamic Therapy, *Adv. Funct. Mater.*, 2022, **32**, 2207749, DOI: 10.1002/adfm.202207749.

50 D. Wang, L. Lin, T. Li, M. Meng, K. Hao, Z. Guo, J. Chen, H. Tian and X. Chen, Etching Bulk Covalent Organic Frameworks into Nanoparticles of Uniform and Controllable Size by the Molecular Exchange Etching Method for Sonodynamic and Immune Combination Antitumor Therapy, *Adv. Mater.*, 2022, **34**, 2205924, DOI: 10.1002/adma.202205924.

51 L. Zhang, Y. Xiao, Q.-C. Yang, L.-L. Yang, S.-C. Wan, S. Wang, L. Zhang, H. Deng and Z.-J. Sun, Staggered Stacking Covalent Organic Frameworks for Boosting Cancer Immunotherapy, *Adv. Funct. Mater.*, 2022, **32**, 2201542, DOI: 10.1002/adfm.202201542.

52 L. Zhang, Q.-C. Yang, S. Wang, Y. Xiao, S.-C. Wan, H. Deng and Z.-J. Sun, Engineering Multienzyme-Mimicking Covalent Organic Frameworks as Pyroptosis Inducers for Boosting Antitumor Immunity, *Adv. Mater.*, 2022, **34**, 2108174, DOI: 10.1002/adma.202108174.

53 Y. Zhang, J. Sheng, F. Zhai, X. Wang, L. Chen, C. Shi, L. Chen, L. He, R. Bai, J. Xie, Z. Chai and J. Diwu, Pioneering Iodine-125-Labeled Nanoscale Covalent Organic Frameworks for Brachytherapy, *Bioconjugate Chem.*, 2021, **32**, 755–762, DOI: 10.1021/acs.bioconjchem.1c00040.

54 L. Feng, C. Qian and Y. Zhao, Recent Advances in Covalent Organic Framework-Based Nanosystems for Bioimaging and Therapeutic Applications, *ACS Mater. Lett.*, 2020, **2**, 1074–1092, DOI: 10.1021/acsmaterialslett.0c00260.

55 Q. Guan, L.-L. Zhou, W.-Y. Li, Y.-A. Li and Y.-B. Dong, Covalent Organic Frameworks (COFs) for Cancer Therapeutics, *Chem.–Eur. J.*, 2020, **26**, 5583–5591, DOI: 10.1002/chem.201905150.

56 S. Li, J. Zou, L. Tan, Z. Huang, P. Liang and X. Meng, Covalent Organic Frameworks: From Linkages to Biomedical Applications, *Chem. Eng. J.*, 2022, **446**, 137148, DOI: 10.1016/j.cej.2022.137148.

57 Q. Guan, L.-L. Zhou and Y.-B. Dong, Construction of Covalent Organic Frameworks via Multicomponent Reactions, *J. Am. Chem. Soc.*, 2023, **145**, 1475–1496, DOI: 10.1021/jacs.2c11071.

58 L.-L. Zhou, Q. Guan, W. Zhou, J.-L. Kan and Y.-B. Dong, Ambient Synthesis of an Iminium-Linked Covalent Organic Framework for Synergetic RNA Interference and Metabolic Therapy of Fibrosarcoma, *Chem. Sci.*, 2022, **13**, 7846–7854, DOI: 10.1039/D2SC02297D.

59 H. L. Nguyen, Reticular Design and Crystal Structure Determination of Covalent Organic Frameworks, *Chem. Sci.*, 2021, **12**, 8632–8647, DOI: 10.1039/D1SC00738F.

60 S.-L. Cai, Z.-H. He, X.-L. Li, K. Zhang, S.-R. Zheng, J. Fan, Y. Liu and W.-G. Zhang, An Unprecedented 2D Covalent Organic Framework with an htb Net Topology, *Chem. Commun.*, 2019, **55**, 13454–13457, DOI: 10.1039/C9CC06780A.

61 S.-Y. Jiang, S.-X. Gan, X. Zhang, H. Li, Q.-Y. Qi, F.-Z. Cui, J. Lu and X. Zhao, Aminal-Linked Covalent Organic Frameworks through Condensation of Secondary Amine with Aldehyde, *J. Am. Chem. Soc.*, 2019, **141**, 14981–14986, DOI: 10.1021/jacs.9b08017.

62 B. Hourahine, B. Aradi, V. Blum, F. Bonafé, A. Buccheri, C. Camacho, C. Cevallos, M. Y. Deshaye, T. Dumitrică, A. Dominguez, S. Ehlert, M. Elstner, T. van der Heide, J. Hermann, S. Irle, J. J. Kranz, C. Köhler, T. Kowalczyk, T. Kubař, I. S. Lee, V. Lutsker, R. J. Maurer, S. K. Min, I. Mitchell, C. Negre, T. A. Niehaus, A. M. N. Niklasson, A. J. Page, A. Pecchia, G. Penazzi, M. P. Persson, J. Řezáč, C. G. Sánchez, M. Sternberg, M. Stöhr, F. Stuckenberg, A. Tkatchenko, V. W. z. Yu and T. Frauenheim, DFTB+, a Software Package for Efficient Approximate Density Functional Theory Based Atomistic Simulations, *J. Chem. Phys.*, 2020, **152**, 124101, DOI: 10.1063/1.5143190.

63 S. Haldar, R. Kushwaha, R. Maity and R. Vaidhyanathan, Pyridine-Rich Covalent Organic Frameworks as High-Performance Solid-State Supercapacitors, *ACS Mater. Lett.*, 2019, **1**, 490–497, DOI: 10.1021/acsmaterialslett.9b00222.

64 J. Li, J. Wang, Z. Wu, S. Tao and D. Jiang, Ultrafast and Stable Proton Conduction in Polybenzimidazole Covalent Organic Frameworks via Confinement and Activation, *Angew. Chem., Int. Ed.*, 2021, **60**, 12918–12923, DOI: 10.1002/anie.202101400.

65 T. K. Dutta and A. Patra, Post-Synthetic Modification of Covalent Organic Frameworks through In Situ Polymerization of Aniline for Enhanced Capacitive Energy Storage, *Chem.–Asian J.*, 2021, **16**, 158–164, DOI: 10.1002/asia.202001216.

66 C. Kang, Z. Zhang, A. K. Usadi, D. C. Calabro, L. S. Baugh, K. Yu, Y. Wang and D. Zhao, Aggregated Structures of Two-Dimensional Covalent Organic Frameworks, *J. Am. Chem. Soc.*, 2022, **144**, 3192–3199, DOI: 10.1021/jacs.1c12708.

67 K. A. Cychosz, R. Guillet-Nicolas, J. García-Martínez and M. Thommes, Recent Advances in the Textural Characterization of Hierarchically Structured Nanoporous Materials, *Chem. Soc. Rev.*, 2017, **46**, 389–414, DOI: 10.1039/C6CS00391E.

68 H. Xu, S. Tao and D. Jiang, Proton Conduction in Crystalline and Porous Covalent Organic Frameworks, *Nat. Mater.*, 2016, **15**, 722–726, DOI: 10.1038/nmat4611.

69 J. Yang, A. Acharjya, M.-Y. Ye, J. Rabeah, S. Li, Z. Kochovski, S. Youk, J. Roeser, J. Grüneberg, M. Schwarze, T. Wang, Y. Lu, R. van de Krol, M. Oschatz, R. Schomäcker, P. Saalfrank, A. Thomas and C. Penschke, Protonated Imine-Linked Covalent Organic Frameworks for

Photocatalytic Hydrogen Evolution, *Angew. Chem., Int. Ed.*, 2021, **60**, 19797–19803, DOI: 10.1002/anie.202104870.

70 R. Kushwaha, S. Haldar, P. Shekhar, A. Krishnan, J. Saha, P. Hui, C. P. Vinod, C. Subramaniam and R. Vaidhyanathan, Exceptional Capacitance Enhancement of a Non-Conducting COF through Potential-Driven Chemical Modulation by Redox Electrolyte, *Adv. Energy Mater.*, 2021, **11**, 2003626, DOI: 10.1002/aenm.202003626.

71 Y. Xie, T. Pan, Q. Lei, C. Chen, X. Dong, Y. Yuan, W. A. Maksoud, L. Zhao, L. Cavallo, I. Pinnau and Y. Han, Efficient and Simultaneous Capture of Iodine and Methyl Iodide Achieved by a Covalent Organic Framework, *Nat. Commun.*, 2022, **13**, 2878, DOI: 10.1038/s41467-022-30663-3.

72 T. Liu, Y. Zhao, M. Song, X. Pang, X. Shi, J. Jia, L. Chi and G. Lu, Ordered Macro–Microporous Single Crystals of Covalent Organic Frameworks with Efficient Sorption of Iodine, *J. Am. Chem. Soc.*, 2023, **145**, 2544–2552, DOI: 10.1021/jacs.2c12284.

73 K. E. deKrafft, W. S. Boyle, L. M. Burk, O. Z. Zhou and W. Lin, Zr- and Hf-Based Nanoscale Metal-Organic Frameworks as Contrast Agents for Computed Tomography, *J. Mater. Chem.*, 2012, **22**, 18139–18144, DOI: 10.1039/C2JM32299D.

74 Q. Yin, F. Y. Yap, L. Yin, L. Ma, Q. Zhou, L. W. Dobrucki, T. M. Fan, R. C. Gaba and J. Cheng, Poly(iohexol) Nanoparticles As Contrast Agents for In Vivo X-ray Computed Tomography Imaging, *J. Am. Chem. Soc.*, 2013, **135**, 13620–13623, DOI: 10.1021/ja405196f.

75 L. Bai, W. Yi, J. Chen, B. Wang, Y. Tian, P. Zhang, X. Cheng, J. Si, X. Hou and J. Hou, Two-Stage Targeted Bismuthene-Based Composite Nanosystem for Multimodal Imaging Guided Enhanced Hyperthermia and Inhibition of Tumor Recurrence, *ACS Appl. Mater. Interfaces*, 2022, **14**, 25050–25064, DOI: 10.1021/acsami.2c01128.

76 I. Noh, D. Lee, H. Kim, C.-U. Jeong, Y. Lee, J.-O. Ahn, H. Hyun, J.-H. Park and Y.-C. Kim, Enhanced Photodynamic Cancer Treatment by Mitochondria-Targeting and Brominated Near-Infrared Fluorophores, *Adv. Sci.*, 2018, **5**, 1700481, DOI: 10.1002/advs.201700481.

77 M. L. Read, K. Brookes, C. E. M. Thornton, A. Fletcher, H. R. Nieto, M. Alshahrani, R. Khan, P. Borges de Souza, L. Zha, J. R. M. Webster, L. J. Alderwick, M. J. Campbell, K. Boelaert, V. E. Smith and C. J. McCabe, Targeting Non-Canonical Pathways as a Strategy to Modulate the Sodium Iodide Symporter, *Cell Chem. Biol.*, 2022, **29**, 502–516, DOI: 10.1016/j.chembiol.2021.07.016.

78 L. Van der Meeren, J. Verduijn, D. V. Krysko and A. G. Skirtach, AFM Analysis Enables Differentiation between Apoptosis, Necroptosis, and Ferroptosis in Murine Cancer Cells, *iScience*, 2020, **23**, 101816, DOI: 10.1016/j.isci.2020.101816.

79 L. Tirinato, M. G. Marafioti, F. Pagliari, J. Jansen, I. Aversa, R. Hanley, C. Nisticò, D. Garcia-Calderón, G. Genard, J. F. Guerreiro, F. S. Costanzo and J. Seco, Lipid Droplets and Ferritin Heavy Chain: A Devilish Liaison in Human Cancer Cell Radioresistance, *eLife*, 2021, **10**, e72943, DOI: 10.7554/elife.72943.

80 R. Chen, Z. Li, C. Peng, L. Wen, L. Xiao and Y. Li, Rational Design of Novel Lipophilic Aggregation-Induced Emission Probes for Revealing the Dynamics of Lipid Droplets during Lipophagy and Ferroptosis, *Anal. Chem.*, 2022, **94**, 13432–13439, DOI: 10.1021/acs.analchem.2c02260.

81 F. Natale, A. Rapp, W. Yu, A. Maiser, H. Harz, A. Scholl, S. Grulich, T. Anton, D. Hörl, W. Chen, M. Durante, G. Taucher-Scholz, H. Leonhardt and M. C. Cardoso, Identification of the Elementary Structural Units of the DNA Damage Response, *Nat. Commun.*, 2017, **8**, 15760, DOI: 10.1038/ncomms15760.

82 L.-L. Zhou, Q. Guan, W.-Y. Li, Z. Zhang, Y.-A. Li and Y.-B. Dong, A Ferrocene-Functionalized Covalent Organic Framework for Enhancing Chemodynamic Therapy via Redox Dyshomeostasis, *Small*, 2021, **17**, 2101368, DOI: 10.1002/smll.202101368.

83 S. Zhang, S. Xia, L. Chen, Y. Chen and J. Zhou, Covalent Organic Framework Nanobowls as Activatable Nanosensitizers for Tumor-Specific and Ferroptosis-Augmented Sonodynamic Therapy, *Adv. Sci.*, 2023, **10**, 2206009, DOI: 10.1002/advs.202206009.

84 B. R. Stockwell, Ferroptosis Turns 10: Emerging Mechanisms, Physiological Functions, and Therapeutic Applications, *Cell*, 2022, **185**, 2401–2421, DOI: 10.1016/j.cell.2022.06.003.

85 X. Chen, R. Kang, G. Kroemer and D. Tang, Ferroptosis in Infection, Inflammation, and Immunity, *J. Exp. Med.*, 2021, **218**, e20210518, DOI: 10.1084/jem.20210518.

86 M. Soula, R. A. Weber, O. Zilka, H. Alwaseem, K. La, F. Yen, H. Molina, J. Garcia-Bermudez, D. A. Pratt and K. Birsoy, Metabolic Determinants of Cancer Cell Sensitivity to Canonical Ferroptosis Inducers, *Nat. Chem. Biol.*, 2020, **16**, 1351–1360, DOI: 10.1038/s41589-020-0613-y.

87 L. F. Ye, K. R. Chaudhary, F. Zandkarimi, A. D. Harken, C. J. Kinslow, P. S. Upadhyayula, A. Dovas, D. M. Higgins, H. Tan, Y. Zhang, M. Buonanno, T. J. C. Wang, T. K. Hei, J. N. Bruce, P. D. Canoll, S. K. Cheng and B. R. Stockwell, Radiation-Induced Lipid Peroxidation Triggers Ferroptosis and Synergizes with Ferroptosis Inducers, *ACS Chem. Biol.*, 2020, **15**, 469–484, DOI: 10.1021/acschembio.9b00939.

88 X. Lang, M. D. Green, W. Wang, J. Yu, J. E. Choi, L. Jiang, P. Liao, J. Zhou, Q. Zhang, A. Dow, A. L. Saripalli, I. Kryczek, S. Wei, W. Szeliga, L. Vatan, E. M. Stone, G. Georgiou, M. Cieslik, D. R. Wahl, M. A. Morgan, A. M. Chinnaiyan, T. S. Lawrence and W. Zou, Radiotherapy and Immunotherapy Promote Tumoral Lipid Oxidation and Ferroptosis via Synergistic Repression of SLC7A11, *Cancer Discov.*, 2019, **9**, 1673–1685, DOI: 10.1158/2159-8290.CD-19-0338.

89 G. Lei, Y. Zhang, P. Koppula, X. Liu, J. Zhang, S. H. Lin, J. A. Ajani, Q. Xiao, Z. Liao, H. Wang and B. Gan, The Role of Ferroptosis in Ionizing Radiation-Induced Cell Death and Tumor Suppression, *Cell Res.*, 2020, **30**, 146–162, DOI: 10.1038/s41422-019-0263-3.

90 Q. Guan, L.-L. Zhou and Y.-B. Dong, Ferroptosis in Cancer Therapeutics: A Materials Chemistry Perspective, *J. Mater. Chem. B*, 2021, **9**, 8906–8936, DOI: 10.1039/D1TB01654G.

91 W.-Y. Li, J.-J. Wan, J.-L. Kan, B. Wang, T. Song, Q. Guan, L.-L. Zhou, Y.-A. Li and Y.-B. Dong, A Biodegradable Covalent Organic Framework for Synergistic Tumor Therapy, *Chem. Sci.*, 2023, **14**, 1453–1460, DOI: **10.1039/D2SC05732H**.

92 Y. Wang, W. Zhen, X. Jiang and J. Li, Driving Forces Sorted In Situ Size-Increasing Strategy for Enhanced Tumor Imaging and Therapy, *Small Sci.*, 2022, **2**, 2100117, DOI: **10.1002/smsc.202100117**.

93 J. Shi, P. W. Kantoff, R. Wooster and O. C. Farokhzad, Cancer Nanomedicine: Progress, Challenges and Opportunities, *Nat. Rev. Cancer*, 2017, **17**, 20–37, DOI: **10.1038/nrc.2016.108**.

94 L. Xie, J. Li, G. Wang, W. Sang, M. Xu, W. Li, J. Yan, B. Li, Z. Zhang, Q. Zhao, Z. Yuan, Q. Fan and Y. Dai, Phototheranostic Metal-Phenolic Networks with Antiexosomal PD-L1 Enhanced Ferroptosis for Synergistic Immunotherapy, *J. Am. Chem. Soc.*, 2022, **144**, 787–797, DOI: **10.1021/jacs.1c09753**.

95 N. Melling, C. M. Kowitz, R. Simon, C. Bokemeyer, L. Terracciano, G. Sauter, J. R. Izbicki and A. H. Marx, High Ki67 Expression is an Independent Good Prognostic Marker in Colorectal Cancer, *J. Clin. Pathol.*, 2016, **69**, 209, DOI: **10.1136/jclinpath-2015-202985**.